scientific reports

Check for updates

OPEN

NADPH oxidase 4 deficiency promotes hepatocellular carcinoma arising from hepatic fibrosis by inducing M2-macrophages in the tumor microenvironment

Ji Young Kim[1,6], Wonseok Kang[1,2,3,4,6], Sera Yang[2], Su Hyun Park[1], Sang Yun Ha[5] & Yong-Han Paik[1,2]✉

Hepatocellular carcinoma (HCC) often arises in the cirrhotic livers, highlighting the intricate link between hepatic fibrosis and carcinogenesis. Reactive oxygen species produced by NADPH oxidase 4 (NOX4) contribute to liver injury leading to hepatic fibrosis. Paradoxically, NOX4 is known to inhibit HCC progression. This study aims to elucidate the role of NOX4 in hepatocarcinogenesis in the background of hepatic fibrosis. We established the mouse model of HCC arising from the fibrotic liver by administering diethylnitrosamine and carbon tetrachloride to wild-type (WT) or NOX4$^{-/-}$ mice. Hepatic fibrogenesis, tumorigenesis, and macrophage polarization were assessed by immunohistochemistry, PCR, and flow cytometry using in vivo and in vitro models. In NOX4$^{-/-}$ mice, hepatic fibrosis was attenuated, while the number of tumors and the proliferation of HCC cells were increased compared to WT mice. Notably, a significant increase in M2-polarized macrophages was observed in NOX4$^{-/-}$ mice through immunohistochemistry and PCR analysis. Subsequent experiments demonstrated that NOX4-silenced HCC cells promote macrophage polarization toward M2. In addition to attenuating hepatic fibrogenesis, NOX4 deficiency triggers macrophage polarization towards the M2 phenotype in the fibrotic liver, thereby promoting hepatocellular carcinogenesis. These findings provide novel insights into the mechanism of NOX4-mediated tumor suppression in HCC arising from fibrotic livers.

Abbreviations

NOX	NADPH oxidase
HCC	Hepatocellular carcinoma
DEN	Diethylnitrosamine
CCl_4	Carbon tetrachloride
KCs	Kupffer cells
HSCs	Hepatic stellate cells
TNFα	Tumor necrosis factor-alpha
AST	Aspartate aminotransferase
ALT	Alanine aminotransferase
CTGF	Connective tissue growth factor
PCNA	Proliferating cell nuclear antigen
AFP	Alpha-fetoprotein
IL	Interleukin
TME	Tumor microenvironment

[1]Department of Health Sciences and Technology, Samsung Advanced Institute of Health Sciences and Technology (SAIHST), Sungkyunkwan University, Seoul 06355, Republic of Korea. [2]Department of Medicine, Samsung Medical Center, Sungkyunkwan University School of Medicine, Seoul 06351, Republic of Korea. [3]Research Institute for Future Medicine, Samsung Medical Center, Seoul 06351, Republic of Korea. [4]Samsung Genome Institute, Samsung Medical Center, Seoul 06351, Republic of Korea. [5]Department of Pathology, Samsung Medical Center, Sungkyunkwan University School of Medicine, Seoul 06351, Republic of Korea. [6]These authors contributed equally: Ji Young Kim and Wonseok Kang. ✉email: yh.paik@skku.edu

Hepatocellular carcinoma (HCC) is the most common type of primary liver cancer and is a leading cause of cancer-related death worldwide[1–3]. Approximately 70–80% of HCC develops within the context of liver cirrhosis[4,5], a terminal stage of hepatic fibrosis. Hepatic fibrosis emerges as a wound-healing response to liver damage instigated by a multitude of factors, encompassing toxic substances, microbial pathogens, or metabolic stressors[6–11]. This intimate link between liver cirrhosis and HCC places them along a shared disease spectrum. However, the intricate mechanisms governing HCC development against a background of hepatic fibrosis remain elusive. Consequently, elucidating this complex interplay is important for both HCC prevention and the development of novel therapeutic strategies.

Oxidative stress, caused by reactive oxygen species (ROS), induces various kinds of liver damage and acts as a significant inducer of hepatic fibrosis[12–14]. Oxidative stress-induced hepatocyte injury leads to inflammatory responses by recruiting immune cells like Kupffer cells (KCs) and activating nonparenchymal cells such as hepatic stellate cells (HSCs). This dysregulated process often fosters the development and progression of HCC[13,15]. Recent studies have shown a positive correlation between chronic IL-6 secretion by inflammatory cells and the progression of HCC[16–19]. ROS, recognized as a critical signal transducer for hepatocarcinogenesis[20,21], attenuates T cell-mediated immune responses within the HCC-associated tumor microenvironment (TME), thereby assuming a pivotal role in hepatocarcinogenesis[22].

Of particular note, NADPH oxidase (NOX) is known as an enzyme responsible for generating ROS in the liver[23]. Previous studies have shown substantial role of NOX-mediated oxidative stress in liver fibrosis across various liver diseases, including alcoholic liver disease, chronic hepatitis C[24,25], and non-alcoholic steatohepatitis[26–28]. Moreover, reports indicate that NOX-mediated oxidative stress affects the mechanism underlying HCC development and shapes the interaction between immune cells and tumor cells within the TME. While NOX1, particularly in hepatic macrophages, has been associated with promoting hepatocarcinogenesis by inducing inflammatory cytokines like IL6 and TNFα[29], it has also been noted that the expression of NOX1 and NOX4 increases in various liver cell types with advanced hepatic fibrosis[26,30].

However, in contrast to NOX1, NOX4 seems to have a tumor-suppressive role in the context of HCC development. Reports have shown that the deficiency of NOX4 in HCC tumor cells fosters HCC progression through metabolic reprogramming[31]. Significantly, our previous study analyzing liver cancer tissues from patients undergoing liver cancer resection revealed a prolonged recurrence-free survival in those exhibiting higher NOX4 expression in their liver cancer tissue[32].

In light of this background, we aimed to investigate the mechanisms through which NOX4 mediates suppression in the context of hepatocellular carcinogenesis arising from a fibrotic background liver. Our primary focus lies in elucidating the intricate interactions between tumor cells and immune cells within the TME.

Results

Absence of NOX4 increases HCC tumorigenesis in the context of hepatic fibrosis

To investigate the impact of NOX4 on tumorigenesis in the context of hepatic fibrosis, we established a mouse model of fibrosis-driven HCC by administering DEN and CCl_4 in WT and NOX4$^{-/-}$ mice (Fig. 1A). Treatment with DEN and CCl_4 induced liver surface nodular changes and the formation of yellow-colored intrahepatic tumor nodules in both WT and NOX4$^{-/-}$ mice (Fig. 1B). There were no significant differences in liver weight-to-body weight ratio, serum AST, and ALT levels between WT and NOX4$^{-/-}$ mice (Fig. 1C). However, NOX4$^{-/-}$ mice exhibited a significantly higher number of tumors, particularly smaller-sized (< 5 mm), compared to WT mice (Fig. 1D). There was no statistical difference in the number of tumors between < 5 mm and 5–10 mm groups within the NOX4 KO mice. These findings suggest an association between NOX4 and the development and growth of HCC.

NOX4 deficiency suppresses hepatic fibrosis but promotes HCC proliferation

To validate our hypothesis regarding the distinct roles of NOX4 in hepatic fibrogenesis and tumorigenesis, we conducted immunohistochemical assays. Hematoxylin/eosin staining of liver tissue encompassing both tumor and non-tumor regions revealed comparable histological features between DEN and CCl_4-treated WT and NOX4$^{-/-}$ mice (Fig. 2A). Interestingly, hepatic fibrosis in the non-tumor regions was notably attenuated in NOX4$^{-/-}$ mice compared to WT mice (Fig. 2B). Furthermore, the mRNA expressions of *Connective Tissue Growth Factor (CTGF)* was reduced in the non-tumor regions of NOX4$^{-/-}$ mice compared to WT mice (Fig. 2C). On the contrary, tumor cell proliferation, as indicated by PCNA-positive cells, was significantly higher in NOX4$^{-/-}$ mice compared to WT mice (Fig. 2D). This increase in proliferation was corroborated by elevated mRNA expressions of *Ki67* and alpha-fetoprotein (*Afp*) in the tumor regions of NOX4$^{-/-}$ mice (Fig. 2E). Similar findings were observed in in vitro cell proliferation assay using NOX4-silenced human HCC cell lines, which exhibited significantly increased cell proliferation rates compared to the control (Fig. 2F). These results suggest that NOX4 deficiency attenuates hepatic fibrosis but promotes the development and progression of HCC, underlining a distinct role for NOX4 in hepatic fibrogenesis and tumorigenesis.

Increased M2-type tumor-associated macrophages (TAMs) in NOX4$^{-/-}$ mice

Macrophage polarization has been shown to influence various aspects of tumor development, including proliferation and resistance against anti-cancer treatments[33]. To elucidate why NOX4 deficiency is associated with reduced hepatic fibrosis but increased tumorigenesis, we focused on the role of macrophages in the TME. Immunohistochemistry of tumor tissues revealed an increase of tumor-associated macrophages (TAMs) in both NOX4$^{-/-}$ and WT mice (Fig. 3A). Similarly, mRNA expression of *CD68* and *Adgre1*, markers for TAMs, was increased (Fig. 3B). Notably, CD206, a representative marker for M2-polarized TAMs, was elevated in tumors of NOX4$^{-/-}$ mice (Fig. 3C), and mRNA expression of *MRC1* further supported the presence of M2-polarized TAMs

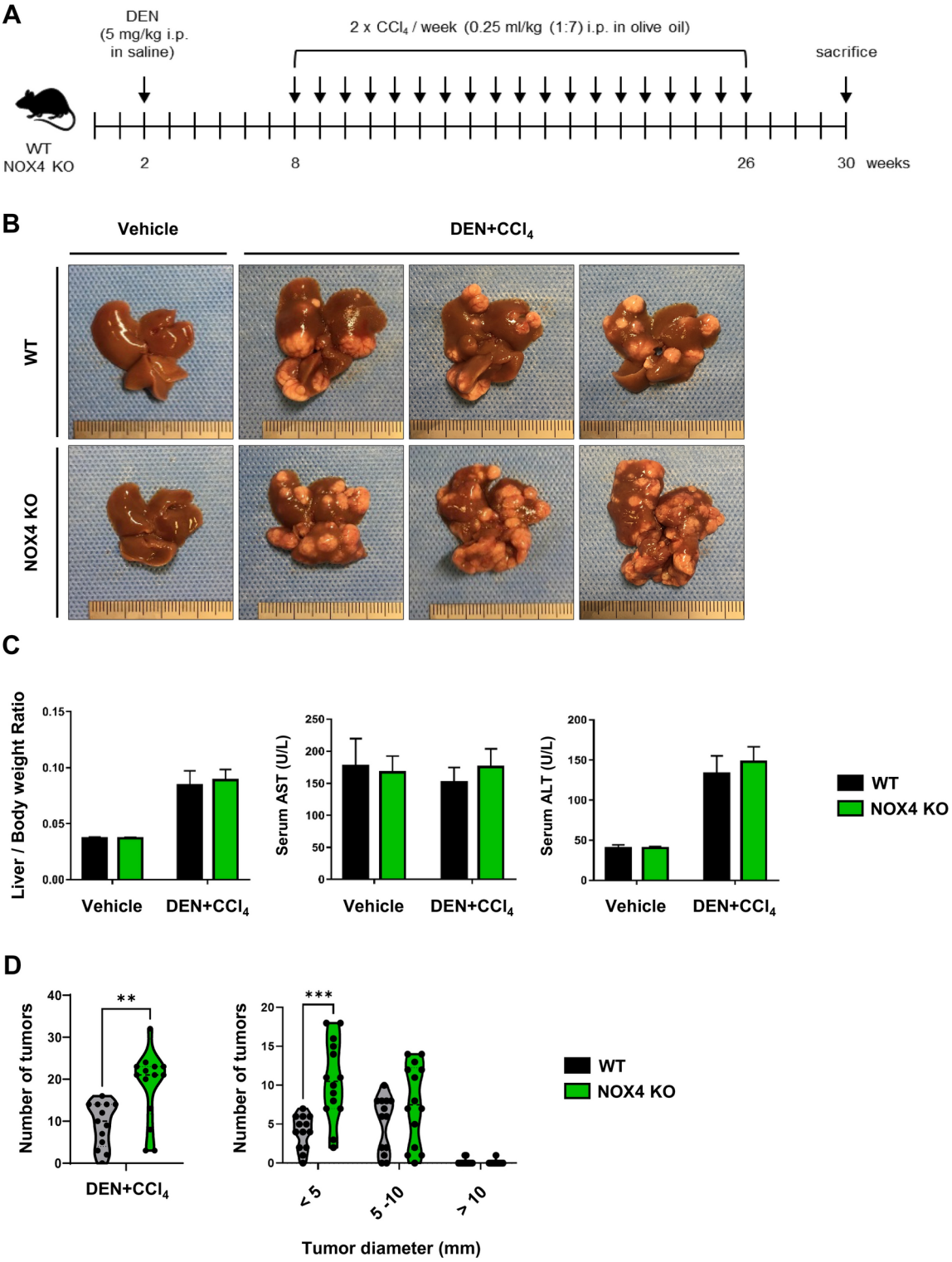

Fig. 1. Absence of NOX4 increases HCC tumorigenesis in a fibrotic background liver. (**A**) Scheme representation of the experimental design for the HCC model, incorporating DEN and CCl_4 injections. (**B**) Representative images of liver specimens. (**C**) Liver-to-body weight ratio (LW/BW) and serum AST and ALT levels measured at the time of sacrifice. (**D**) Total tumor numbers in mice injected with DEN and CCl_4 (left), categorized based on tumor diameter (right). No tumors were observed in the control group. Data are shown as mean ± standard error of the mean. Statistical significance was determined using a two-way ANOVA. $^{*}p < 0.05$, $^{**}p < 0.01$.

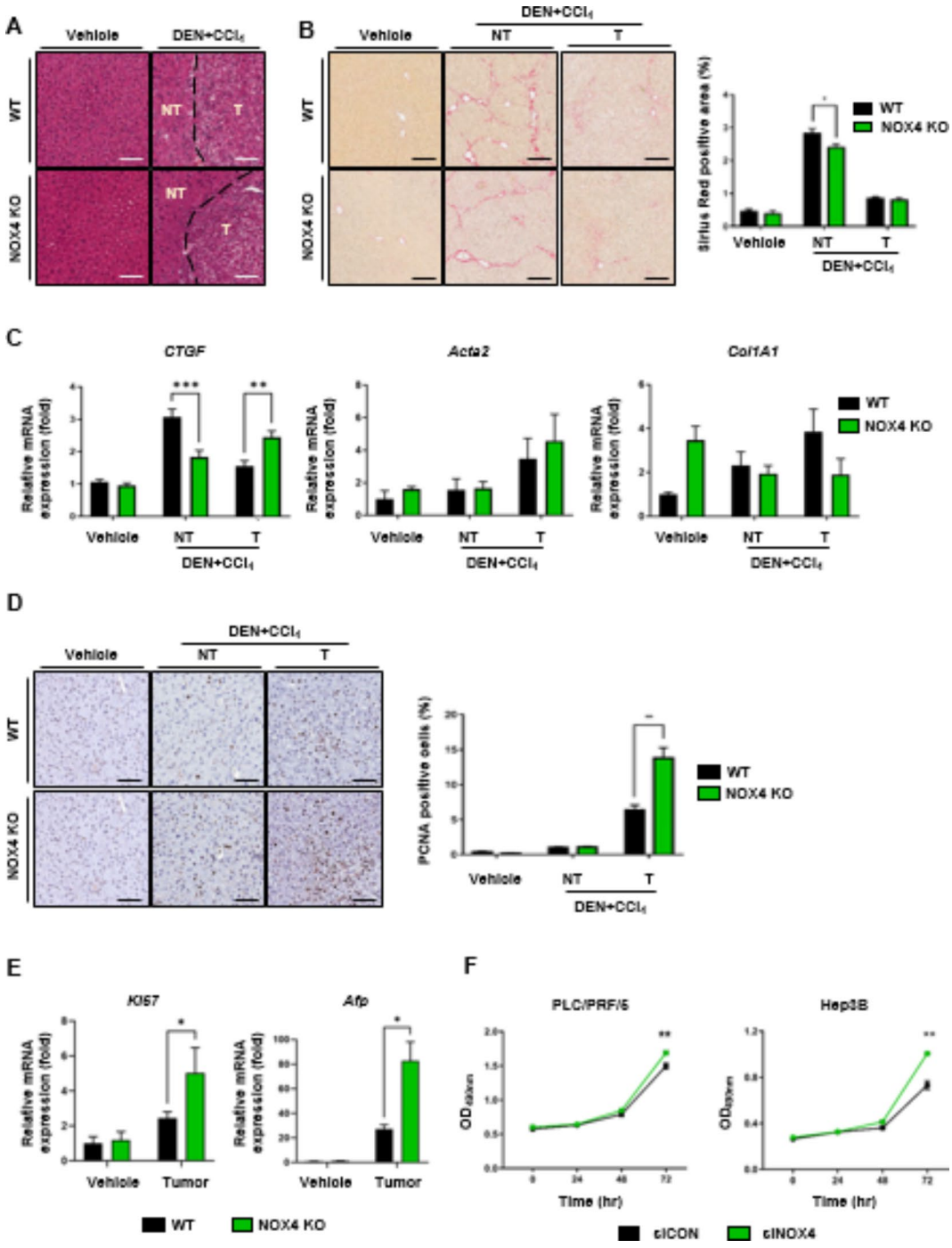

Fig. 2. Role of NOX4 depletion in hepatic fibrosis attenuation and tumor proliferation. (**A**) Representative images of liver sections from mice treated with vehicle or DEN plus CCl_4, stained with Hematoxylin/Eosin (scale bar: 200 μm). Tumor border regions are marked as non-tumor (NT) and tumor (T). (**B**) Representative images of Sirius red staining (left, scale bar: 400 μm) and quantification (right). Positive-staining areas in liver sections from DEN plus CCl_4-treated mice were analyzed in non-tumor (NT) and tumor (T) regions. (**C**) Relative mRNA levels of fibrosis-related genes (*CTGF, Acta2,* and *Col1A1)* in the livers of WT or $NOX4^{-/-}$ mice after DEN and CCl_4 treatment, as determined by quantitative real-time PCR. Data are shown as fold mRNA induction compared with WT vehicle mice, using *GAPDH* as an endogenous control. (**D**) Representative images of proliferating cell nuclear antigen (PCNA) staining (left, scale bar: 200 μm) and the percentage of PCNA-positive-stained cells (right) in non-tumor (NT) and tumor (T) regions of liver sections from DEN and CCl_4-treated mice. (**E**) Relative mRNA levels of *Ki67* and *Afp* in the livers of WT or $NOX4^{-/-}$ mice after DEN and CCl_4 treatment, determined by quantitative real-time PCR. Data are shown as fold mRNA induction compared with WT vehicle mice, using *GAPDH* as an endogenous control. (**F**) Cell proliferation of human HCC cell lines treated with si*NOX4*, assessed by MTS assay. Data are shown as mean ± standard error of the mean. Statistical significance was determined using a two-way ANOVA. $^{*}p < 0.05$, $^{**}p < 0.01$, $^{***}p < 0.005$.

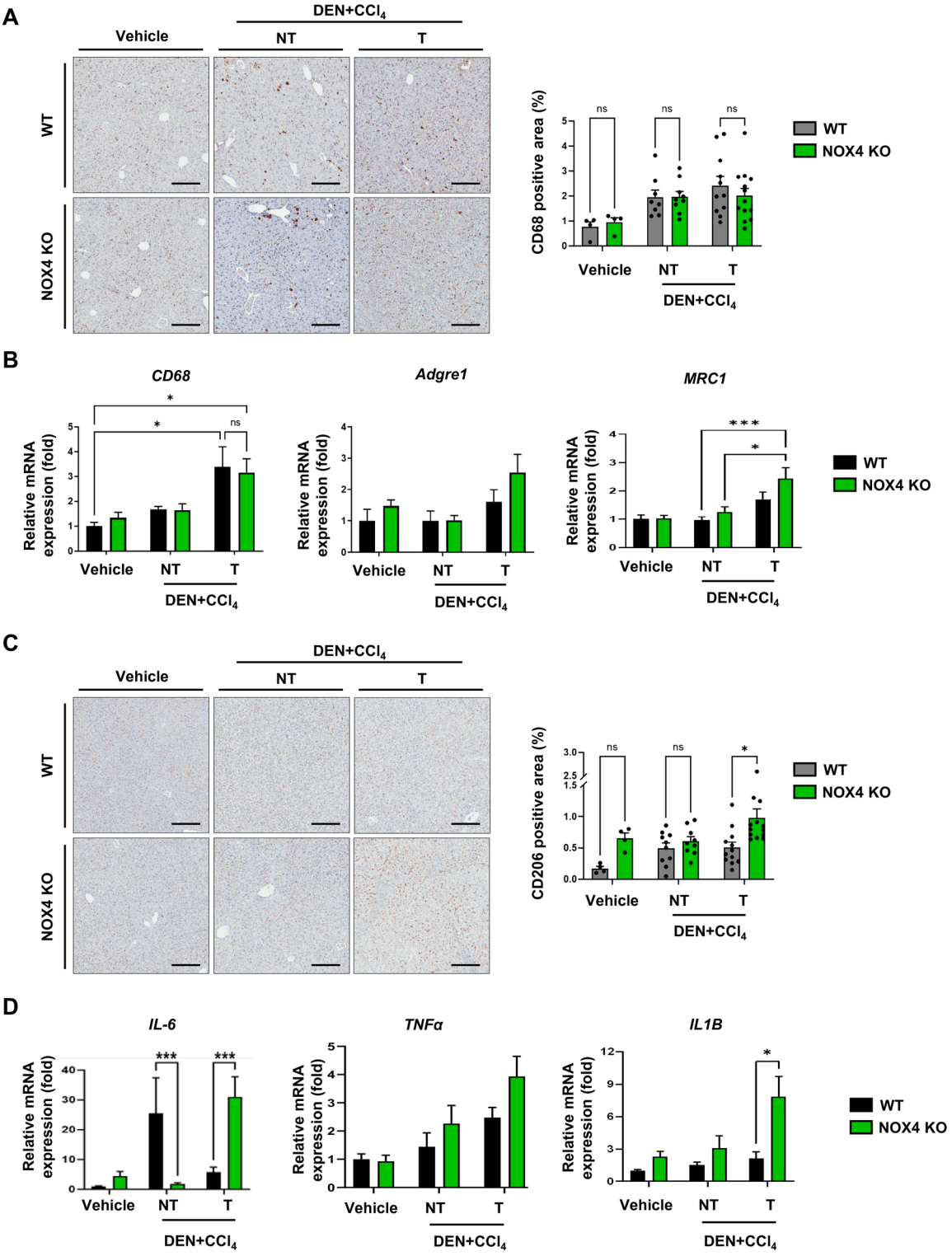

Fig. 3. Impact of NOX4 deficiency on liver inflammation and M2-type macrophages. (**A**) Representative images of CD68 immunohistochemistry staining (left, scale bar: 200 μm) and its quantification (right). (**B**) Relative mRNA levels of immune cell markers (*CD68, Adgre1*, and *MRC1)* in the livers of WT and NOX4$^{-/-}$ mice after DEN and CCl_4 treatment, measured by quantitative real-time PCR. (**C**) Representative images of CD206 immunohistochemistry staining (left, scale bar: 200 μm) and its quantification (right). (**D**) Relative mRNA levels of pro-inflammatory genes (*IL-6, TNFa*) and anti-inflammatory genes (*IL1B)* in the livers of WT and NOX4$^{-/-}$ mice after DEN and CCl_4 treatment, assessed by quantitative real-time PCR. Data are shown as fold mRNA induction compared with WT vehicle mice, using *GAPDH* as an endogenous control. Data are shown as mean ± standard error of the mean. Statistical significance was determined using a two-way ANOVA. $^{*}p < 0.05$, $^{**}p < 0.01$.

(Fig. 3B). Given the reported positive correlation between inflammatory cytokines such as IL-6 and TNFα with HCC progression[34–36], mRNA expression of these inflammatory cytokines was analyzed (Fig. 3D). While *IL6* mRNA levels were reduced in non-tumor tissues of NOX4$^{-/-}$ mice, they were increased in tumor tissues from NOX4$^{-/-}$ mice compared to WT mice. Additionally, mRNA expression of *TNFa* and *IL1B* was also increased in tumor tissues of NOX4$^{-/-}$ mice. Taken together, these findings suggest that the absence of NOX4 results in macrophage polarization towards M2-type TAMs, ultimately promoting HCC tumorigenesis and progression.

NOX4 deficiency leads to M2-polarization of myeloid cells upon liver injury with DEN and CCl_4

To examine the effects of NOX4 on immune cells and tumorigenic responses in the liver, liver injury was induced using DEN and CCl_4 to simulate early-stage hepatic carcinogenesis (Fig. 4A). Intrahepatic mononuclear cells were subsequently isolated and analyzed using multi-color flow cytometry (Fig. 4B). Intrahepatic myeloid cells in the liver demonstrated an increasing trend upon DEN and CCl_4 administration (Fig. 4C). Particularly, the frequency of Kupffer cells (Ly6C$^+$CD11b^{mid}F4/80^{high}) was increased in NOX4$^{-/-}$ mice compared to WT mice. Notably, M1-polarized myeloid cells were reduced in NOX4$^{-/-}$ mice (Fig. 4D), whereas M2-polarized myeloid cells were significantly increased in NOX4$^{-/-}$ mice compared to WT mice (Fig. 4E), resulting in an increased M2/M1 ratio (Fig. 4F). These results suggest that NOX4 deficiency influences the polarization of myeloid cells toward the M2 phenotype upon liver injury induced by DEN and CCl_4.

NOX4-deficient HCC cells promote the polarization of monocyte-derived macrophages to M2-type

To investigate whether NOX4 impacts the polarization of myeloid cells in the TME, mouse bone marrow-derived macrophages (BMDMs) were exposed to the conditioned media from NOX4-silenced human HCC cell lines. Subsequently, flow cytometry was performed to analyze macrophage polarization (Fig. 5A). The results indicated a significant increase in the frequency of CD11b$^+$F4/80$^+$CD206$^+$ cells, as well as the M2/M1 ratio, upon exposure to conditioned media from NOX4-silenced HCC cells (Fig. 5B and C). Similar findings were observed when human monocyte-derived macrophages, induced from THP-1 cells, were exposed to conditioned media from NOX4-silenced human HCC cell lines (Fig. 5C). Exposure to conditioned media from NOX4-silenced human HCC cells led to an increase in M2-polarized macrophages (Fig. 5D). These results suggest that NOX4-deficient HCC cells indirectly promote the polarization of macrophages towards the M2 phenotype in the TME.

Discussion

Liver injury, particularly when triggered by ROS generated by NOX homologs, plays a pivotal role in activating hepatic stellate cells and subsequently leads to hepatic fibrosis, as well as the initiation and progression of HCC[10,11,26]. Nevertheless, the intricate molecular mechanisms underlying the progression from hepatic fibrosis to HCC carcinogenesis remain largely unknown. Our study demonstrates the tumor-suppressive role of NOX4 in the context of HCC development from a fibrotic liver background.

Liver injury caused by ROS generated by NOX homologs serves as a trigger for hepatic inflammation and the innate immune response within the liver, ultimately leading to the activation of HSC and the accumulation of ECM, which in turn contributes to liver fibrosis[26]. Previous studies with chronic CCl_4-administered liver injury model have reported that NOX4 deficiency results in reduced hepatic inflammation, HSC proliferation, and hepatic fibrosis compared to WT mice[37,38]. Paradoxically, the absence of NOX4 appears to promote tumorigenesis and the proliferation of tumor cells. In our study, NOX4$^{-/-}$ mice exhibited diminished hepatic fibrosis and, concurrently, an increased number and size of tumors, following DEN injection and subsequent chronic CCl_4-administration. Moreover, the proliferation of human HCC cell lines silenced for NOX4 by siRNA was notably increased. These results strongly suggest that NOX4 deficiency is associated with an increased incidence of HCC development within the fibrotic liver background. These findings align with our previous reports, which linked lower NOX4 expression to worse survival rates following HCC resection[32].

Recent research underscores the critical role played by the interaction between immune cells and cancer cells in shaping the growth and progression of tumor cells within the TME. The liver contains various immune cells, including a substantial population of macrophages, particularly resident-liver macrophages known as Kupffer cells[39–41]. It has been reported that macrophage-specific *NOX1* knockout mice developed less and smaller HCC compared to WT mice[29]. Furthermore, many studies have revealed the influence of macrophage polarization on various facets of tumor behavior, including development, proliferation, and resistance to anti-cancer drug. Of particular significance, M2-polarized macrophages have been shown to exert a significant impact on HCC cell proliferation and their resistance to sorafenib[33]. In addition, a study identified NOX4 in non-small cell lung cancer cells as a factor influencing macrophage polarization[42]. Given this background, we hypothesized that the reason NOX4 deficiency suppresses hepatic fibrosis but promotes HCC development and growth may be intricately related to macrophage polarization within the HCC TME against the background of hepatic fibrosis. To substantiate our hypothesis, we conducted immunohistochemical staining analysis and gene analysis using mice tissue.

The liver is home to a multitude of immune cells, and accumulating evidence suggests that the interaction between tumor cells and immune cells within the TME plays a pivotal role in tumor initiation and progression[39,43,44]. Among these immune cells, activated macrophages including Kupffer cells, have the capacity to incite a wide range of inflammatory responses by secreting inflammatory cytokines[45–47]. Importantly, macrophages can undergo distinct polarizations, namely M1 and M2, and these polarized macrophages exert diverse effects on inflammation, tissue repair, and tumor survival[48–50]. Likewise, TAMs can significantly influence tumor growth and the TME depending on their polarization. In particular, M2-polarized TAMs are associated with the suppression of immune cell activation and the promotion of tumor proliferation, angiogenesis, and

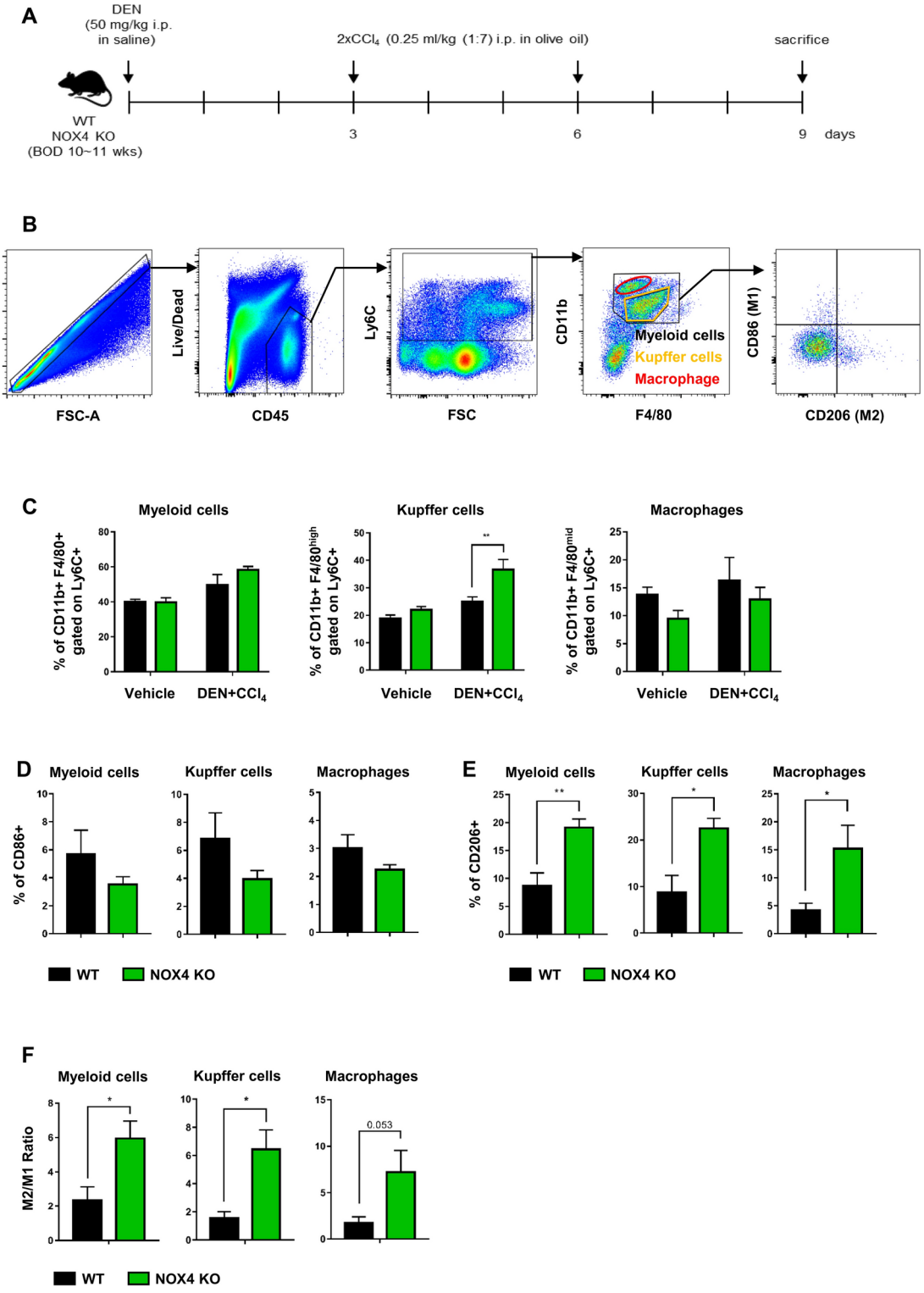

Fig. 4. NOX4 depletion and macrophage polarization in acute inflammatory liver. (**A**) Experimental scheme for the acute inflammatory model using DEN and CCl_4. Mice were treated with DEN injections followed by two CCl_4 injections and were sacrificed 72 h after the final CCl_4 treatment. (**B**) Gating strategy for flow cytometry analysis of leukocytes ($CD45^+$) isolated from liver tissue, stained for myeloid lineage markers and polarization phenotype markers. (**C**–**F**) Flow cytometry analysis of myeloid lineage, including the percentage of $CD11b^+F4/80^{high}$ Kupffer cells and $CD11b^+F4/80^{mid}$ macrophages (**C**), M1-polarized macrophages (**D**), M2-polarized macrophages (**E**), and the M2/M1 ratio (**F**). Data are shown as mean ± standard error of the mean. Statistical significance was determined using a two-way ANOVA. $^*p < 0.05$, $^{**}p < 0.01$.

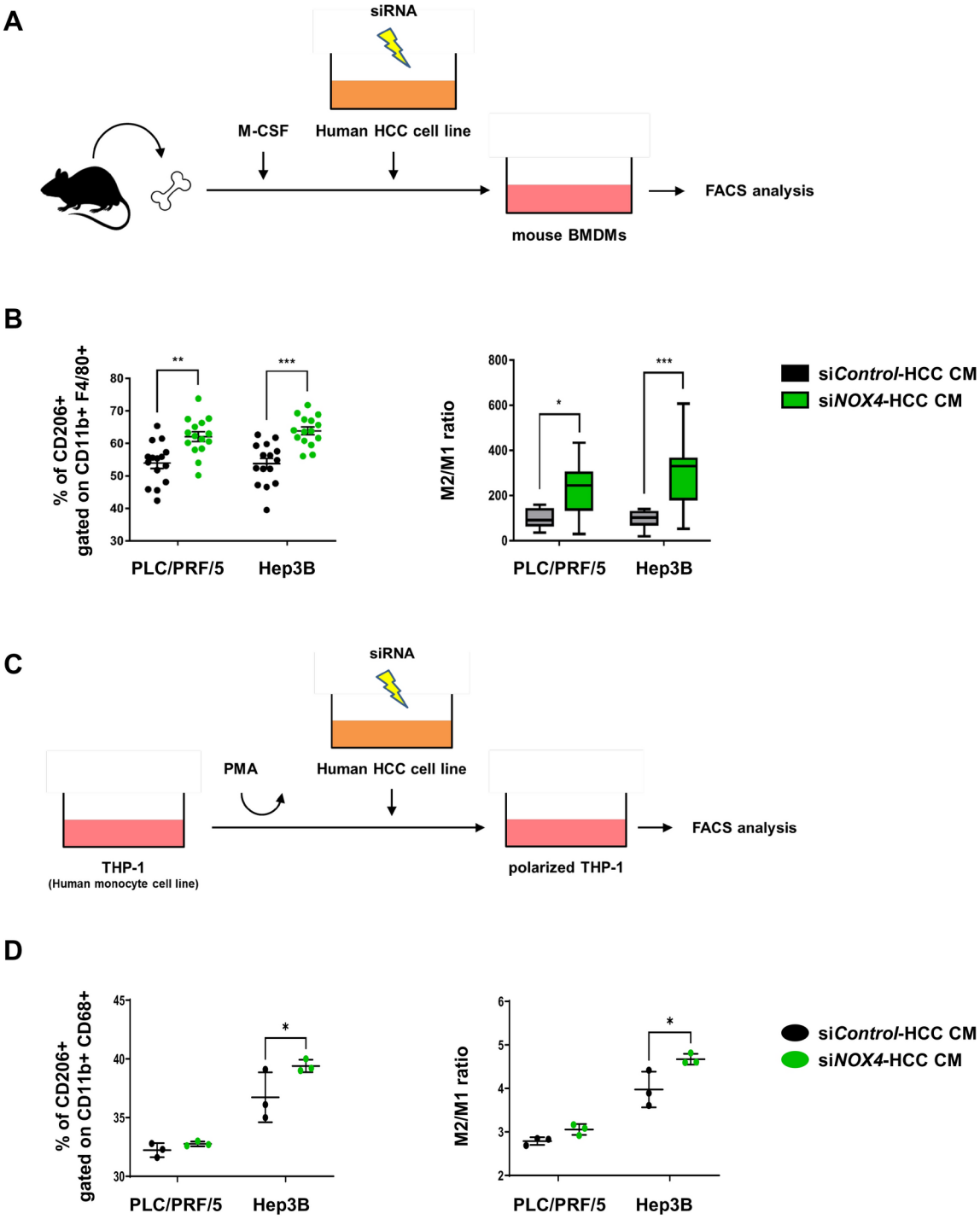

Fig. 5. Impact of NOX4-silencing in HCC on macrophage polarization. (**A**) Experimental scheme for in vitro polarization of mouse bone marrow-derived macrophages (BMDMs). Monocytes from WT mice bone marrow were cultured in conditioned media from siRNA-treated human HCC cell lines. (**B**) Polarization of mouse BMDMs assessed by flow cytometry analysis. (**C**) Experimental scheme for differentiation and polarization of THP-1 cells. Differentiated macrophages were cultured in conditioned media from siRNA-treated human HCC cell line. (**D**) Polarization of THP-1 cells assessed by flow cytometry analysis. Data are shown as mean ± standard error of the mean. Statistical significance was determined using a two-way ANOVA. $^{*}p < 0.05$, $^{**}p < 0.01$.

metastasis[51–53]. In our HCC mouse model within the context of hepatic fibrosis, NOX4-deficient mice exhibited higher expression of M2-polarized macrophage markers, as confirmed by immunohistochemistry staining and mRNA expression analysis. These results indicate that the absence of *NOX4* may function as a tumor promoter by directing macrophages toward a pro-tumoral polarization in the TME.

Next, we investigated macrophage polarization in the context of acute inflammatory liver injury in our mouse model. The results from our acute inflammatory liver model demonstrated a tendency toward an increase in the number of macrophages within the damaged liver following exposure to CCl_4 plus DEN compared to the vehicle group. Interestingly, there was no significant difference NOX4$^{-/-}$ and WT mice. Notably, the population of Kupffer cells (characterized as CD11b^{mid}F4/80^{high}Ly6C^{+} cells) was significantly higher in damaged NOX4$^{-/-}$ mice than in WT counterparts. Furthermore, polarization analysis revealed that Kupffer cells and macrophages in the acute-inflammatory liver were skewed toward the M2 phenotype. Moreover, both mouse primary BMDMs and human monocyte cell lines exhibited a pronounced shift toward M2 polarization in response to conditioned media from *NOX4*-silenced tumor cell lines. Collectively, our data indicate that *NOX4* may act as a tumor suppressor by modulating macrophage polarization with the fibrotic liver. Recent experimental evidence has emphasized the role of M2-polarized TAMs in promoting HCC growth and mediating the TME's resistance to tyrosine kinase inhibitors such as sorafenib[33]. Additionally, M2-like polarization of TAMs has been associated with various malignant behaviors in HCC, including growth, migration, metastasis, and immunosuppression. Our study provides indirect evidence of the involvement of hepatocytes and/or HCC cells in macrophage polarization, and further exploration is warranted to clarify the intricate molecular mechanisms behind the relationship between hepatocytes/HCC cells and polarized macrophages.

In summary, our study introduces a novel perspective in which NOX4 deficiency is intricately linked to macrophage polarization, resulting in the promotion of HCC initiation and development. These findings lay the groundwork for considering NOX4 as a potential tumor suppressor and new therapeutic target arising HCC occurring in the context of liver fibrosis.

Methods

Animal experiments

Inbred male C57BL/6J (wild type, WT) mice and NOX4$^{-/-}$ mice (B6.129-Nox4tm1Kkr/J) were purchased from The Jackson Laboratory (Bar Harbor, Maine, USA). To establish a syngeneic mouse model of HCC in the background of hepatic fibrosis, 5 mg/kg body weight of DEN (Sigma-Aldrich, Saint Louis, MO, USA) or saline was injected intraperitoneally into two-week-old WT or NOX4$^{-/-}$ mice. Six weeks after DEN injection, 0.25 ml/kg of CCl_4 was injected intraperitoneally into the DEN-administrated mice twice a week for 18 weeks. For the control group, an equal amount of olive oil was injected into the saline-administered mice for 18 weeks. For assessment of tumor growth, the mice were euthanasia with 2% isoflurane (Hana Pharm, South Korea) and sacrificed at the end of week 30 after a four-week washout period to eliminate the acute effects of CCl_4. The number of tumor nodules on the surface of the whole liver was counted. Liver tissues were harvested for subsequent analyses including real-time quantitative PCR and immunohistochemistry. Serum aminotransferase levels were measured using Fuji Dri-Chem 3000 (Fujifilm, Tokyo, Japan). For an acute liver injury mouse model, 50 mg/kg of DEN or saline was injected intraperitoneally into 10–11 week-old mice. Three days after DEN injection, 0.25 ml/kg of CCl_4 or olive oil was injected intraperitoneally into the DEN-administered mice twice a week. The mice were sacrificed after 72 h from the last injection, and liver tissues were harvested for multi-color flow cytometry analysis. All methods were performed in accordance with the ARRIVE guidelines and in accordance with the relevant guidelines and regulations. This study was reviewed and approved by the Institutional Animal Care and Use Committee (IACUC) of Samsung Biomedical Research Institute (SBRI). SBRI is an Association for Assessment and Accreditation of Laboratory Animal Care International (AAALAC International) accredited facility and abides by the Institute of Laboratory Animal Resources (ILAR) guide.

Immunohistochemistry

The mouse liver tissues were fixed in 10% neutral buffered formalin (Sigma-Aldrich), embedded in paraffin, and sectioned with 4 μm thickness. Hematoxylin/ eosin or Sirius red staining was performed according to the standard protocol as previously described. For immunohistochemistry (IHC) staining of macrophages in the mouse liver, anti-CD68 antibody (Abcam) and anti-mouse MMR/CD206 antibody (R&D systems) were used as primary antibody. All slides were scanned using Scanscope AT (Aperio, Vista, CA, USA) and analyzed with the Aperio ImageScope software, and quantified with ImageJ (https://imagej.net/ij/, Java 1.8.0_172). Proliferating cell nuclear antigen (PCNA) staining was performed using anti-PCNA antibody (Santa Cruz Biotechnology). The stained slides were scanned and 10 regions of interest (ROI) were selected per slide for quantification. PCNA positivity was calculated as follows: (number of PCNA-positive nuclei)/(total number of nuclei) × 100 (%).

RNA isolation and real-time quantitative PCR

Total RNA was extracted using RNeasy Mini Kit (Qiagen) according to the manufacturer's instructions, and cDNA synthesis was performed using High Capacity RNA-to-cDNA kit (Applied Biosystems). Real-time quantitative PCR (RT-qPCR) was performed using SYBR Green master mix (KAPA). All target gene-specific primers (Bioneer, South Korea) are listed in Supplementary Table S1. The relative gene expression was normalized to GAPDH, calculated using the $2^{-\Delta\Delta CT}$ method, and expressed as fold increases compared to WT.

Cell culture and in vitro experiments

PLC/PRF/5 (American Type Culture Collection [ATCC] Cat# CRL-8024,) and Hep3B (ATCC Cat# CRL-8064) were maintained in DMEM (Welgene, South Korea) with 10% fetal bovine serum (Welgene) and 100 U/ml penicillin–streptomycin (Gibco). THP-1 cells (Korean Cell Line Bank [KCLB] Cat# 40202) were maintained in RPMI-1640 (Welgene) with 10% FBS and 100 U/ml penicillin–streptomycin. For differentiation of THP-1 cells into macrophages, THP-1 cells were cultured in RPMI-1640 containing 10% FBS and 5 ng/ml phorbol 12-myristate 13-acetate (PMA, Sigma-Aldrich) for 24 h. Subsequently, the cells were washed with PBS and

the attached cells were maintained in RPMI-1640 without PMA for three days. Differentiation of THP-1 into macrophages was confirmed by morphological alteration (Supplementary Fig. S1A).

siRNA-mediated gene knockdown in cells

Human HCC cell lines were seeded overnight in a 60-mm culture dish. At 80% confluency, the culture media was replaced with Opti-MEM (Life Technologies) containing a mixture of siRNA of target genes (siNOX4; 5′-CA GAGUAUUUCUCAGAACA-3′, AccuTarget (Negative Control siRNA) and Lipofectamine RNAi/MAX reagent (Life Technologies) according to the manufacturer's instructions. Knockdown of NOX4 was confirmed by RT-qPCR and Western blot (Supplementary Fig. S4). For generation of NOX4-knockdown conditioned media (CM), HCC cells were incubated in DMEM containing 10% FBS for three days after siRNA treatment. After three days, the media was centrifuged, filtered, and stored frozen in aliquots at − 80 ℃ until needed. To evaluate the polarization of macrophages, differentiated THP-1 cells (M0 macrophages) were maintained in the media containing the NOX4-knockdown CM for 72 h (Table 1).

Isolation of primary hepatic mononuclear cells

Primary hepatic mononuclear cells were isolated by ex vivo digestion. Briefly, the mouse livers were cut into small pieces, followed by ex vivo digestion using Enzymatic Dissociation Kit (Miltenyi Biotec) and gentleMACS Octo Dissociator with Heaters (Miltenyi Biotec) according to the manufacturer's instructions. Digested samples were filtered through a 70-μm strainer, and washed with DPBS. Subsequently, the primary hepatic mononuclear cells were isolated by density gradient method using Ficoll-Paque (GE Health Care).

Isolation and polarization of mouse bone marrow-derived macrophages

For isolation of mouse bone marrow-derived macrophages (BMDMs), both tibia and femur were collected from 10 to 11 week-old C57BL/6J mice. After removing the skin and muscles, the bones were washed in 70% ethanol and PBS. Bone marrow cells were harvested by flushing the bone marrow with RPMI-1640. Harvested bone marrow cells were washed in PBS, resuspended in DMEM containing 10% FBS in a petri dish. After 1 day, only the floating cells were harvested and cultured in DMEM containing 10% FBS and 20 ng/ml M-CSF (Peprotech) for 7 days to induce differentiation into BMDMs (Supplementary Fig. S1B). For assessment of the polarization of BMDMs, differentiated BMDMs were exposed to NOX4-knockdown CM for 72 h, followed by flow cytometry analysis.

Flow cytometry analysis

For flow cytometry analysis, the isolated cells were filtered through a round-bottom tube with a 35-μm strainer cap (Falcon). After filtration, the cells were suspended in cold staining buffer containing 1% (v/v) bovine serum albumin (Sigma-Aldrich) and 0.1% sodium azide (Sigma-Aldrich) in PBS. The cells isolated from the mouse liver tissue were stained with LIVE/DEAD Fixable Viability Kit (Invitrogen) and subsequently surface-stained with fluorescent-conjugated antibodies as listed in Table 2. Multi-color flow cytometry was performed using LSRFortessa (BD Biosciences), and the data was analyzed using FlowJo software (BD Life Sciences, version 10.10.0).

Statistical analysis

GraphPad Prism 10 (GraphPad Software, version 10.2) was used for all data analysis in this study. Statistical analyses between 2 groups were carried out by Student's *t* test, with $p < 0.05$ considered as significant. Statistical analyses among 3 or more groups were carried out by ANOVA *t* test, with $p < 0.05$ considered as significant. Error bars were presented as Standard Error of the Mean (SEM).

Gene	Forward primer (5′–3′)	Reverse primer (3′–5′)
GAPDH	AAGGGCTCATGACCACAGTC	CAGGGATGATGTTCTGGGCA
CTGF	ATACGCCTGAGTGGCTGTCT	GGTTCATGTCATGGATGGTG
Acta2	GTTCAGTGGTGCCTCTGTCA	ACTGGGACGACATGGAAAAG
Col1a1	TAGGCCATTGTGTATGCAGC	ACATGTTCAGCTTTGTGGACC
Ki67	CACCTGGTCACCATCAAGC	GCAGCTGGATACGAATGTCA
Afp	GCTCACATCCACGAGGAGTGTT	CAGAAGCCTAGTTGGATCATGGG
CD68	AAGGGGGCTCTTGGGAACTA	ATGCCCCAAGCCTTTCTTCC
Adgre1	CTGTACCTGTCAACCAGGCTT	TGTTGTGGCAGGTTGCATGTT
MRC1	GTTCACCTGGAGTGATGGTTCTC	AGGACATGCCAGGGTCACCTTT
IL-6	AGCTACCTGGAGTACATGAAGA	GTGACTCCAGCTTATCTCTTGGT
TNFα	TGCCTATGTCTCAGCCTCTTC	GAGGCCATTTGGGAACTTCT
IL-1β	GCCACCTTTTGACAGTGATGAG	ATCAGGACAGCCCAGGTCAA

Table 1. Primer sequences for RT-qPCR.

Profiling of immune cells from mouse liver tissue			
Marker	**Fluorochrome**	**Clone**	**Manufacturer**
Anti-mouse CD45	APC-Cy7	30-F11	Biolegend
Anti-mouse Ly6C	PE	HK1.4	Biolegend
Anti-mouse CD11b	PerCP-Cy5.5	M1/70	BD Biosciences
Anti-mouse F4/80	PE-Cy7	BM8	Biolegend
Anti-mouse CD86	BV421	GL-1	Biolegend
Anti-mouse CD206	PE	C068C2	Biolegend
Analysis of macrophage polarization			
Marker	**Fluorochrome**	**Clone**	**Manufacturer**
Anti-mouse CD11b	V500	M1/70	BD Biosciences
Anti-mouse F4/80	Alexa Fluor 488	6F12	BD Biosciences
Anti-mouse CD86	PerCP-Cy5.5	GL-1	Biolegend
Anti-mouse CD206	PE	C068C2	Biolegend
Anti-human CD11b	PerCP	M1/70	Biolegend
Anti-human CD68	FITC	Y1/82A	Biolegend
Anti-human CD86	PE-Cy7	FUN-1	BD Biosciences
Anti-human CD206	APC-Cy7	15-2	Biolegend

Table 2. Fluorochrome-conjugated antibodies for flow cytometry analysis.

Data availability

The data that support the findings of this study are available from the corresponding author upon reasonable request.

Received: 3 December 2023; Accepted: 10 September 2024
Published online: 27 September 2024

References

1. Llovet, J. M. *et al.* Hepatocellular carcinoma. *Nat. Rev. Dis. Primers* **7**, 6. https://doi.org/10.1038/s41572-020-00240-3 (2021).
2. Renne, S. L. & Di Tommaso, L. A clinical and pathological update on hepatocellular carcinoma. *J. Liver Cancer* **22**, 14–22. https://doi.org/10.17998/jlc.2022.03.18 (2022).
3. McGlynn, K. A., Petrick, J. L. & El-Serag, H. B. Epidemiology of hepatocellular carcinoma. *Hepatology* **73**(Suppl 1), 4–13. https://doi.org/10.1002/hep.31288 (2021).
4. El-Serag, H. B. Hepatocellular carcinoma. *N. Engl. J. Med.* **365**, 1118–1127. https://doi.org/10.1056/NEJMra1001683 (2011).
5. Heimbach, J. K. *et al.* AASLD guidelines for the treatment of hepatocellular carcinoma. *Hepatology* **67**, 358–380. https://doi.org/10.1002/hep.29086 (2018).
6. Kisseleva, T. & Brenner, D. Molecular and cellular mechanisms of liver fibrosis and its regression. *Nat. Rev. Gastroenterol. Hepatol.* **18**, 151–166. https://doi.org/10.1038/s41575-020-00372-7 (2021).
7. Aydin, M. M. & Akcali, K. C. Liver fibrosis. *Turk. J. Gastroenterol.* **29**, 14–21. https://doi.org/10.5152/tjg.2018.17330 (2018).
8. Hernandez-Gea, V. & Friedman, S. L. Pathogenesis of liver fibrosis. *Annu. Rev. Pathol.* **6**, 425–456. https://doi.org/10.1146/annurev-pathol-011110-130246 (2011).
9. Wynn, T. A. & Ramalingam, T. R. Mechanisms of fibrosis: Therapeutic translation for fibrotic disease. *Nat. Med.* **18**, 1028–1040. https://doi.org/10.1038/nm.2807 (2012).
10. Bataller, R. & Brenner, D. A. Liver fibrosis. *J. Clin. Investig.* **115**, 209–218. https://doi.org/10.1172/jci24282 (2005).
11. Friedman, S. L. Mechanisms of hepatic fibrogenesis. *Gastroenterology* **134**, 1655–1669. https://doi.org/10.1053/j.gastro.2008.03.003 (2008).
12. Cichoż-Lach, H. & Michalak, A. Oxidative stress as a crucial factor in liver diseases. *World J. Gastroenterol.* **20**, 8082–8091. https://doi.org/10.3748/wjg.v20.i25.8082 (2014).
13. Ramos-Tovar, E. & Muriel, P. Molecular mechanisms that link oxidative stress, inflammation, and fibrosis in the liver. *Antioxidants* **9**, 1279. https://doi.org/10.3390/antiox9121279 (2020).
14. Li, S. *et al.* the role of oxidative stress and antioxidants in liver diseases. *Int. J. Mol. Sci.* **16**, 26087–26124. https://doi.org/10.3390/ijms161125942 (2015).
15. Tarao, K. *et al.* Inflammation in background cirrhosis evokes malignant progression in HCC development from HCV-associated liver cirrhosis. *Scand. J. Gastroenterol.* **48**, 729–735. https://doi.org/10.3109/00365521.2013.782064 (2013).
16. Zheng, X. *et al.* IL-6/STAT3 axis initiated CAFs via up-regulating TIMP-1 which was attenuated by acetylation of STAT3 induced by PCAF in HCC microenvironment. *Cell. Signal.* **28**, 1314–1324. https://doi.org/10.1016/j.cellsig.2016.06.009 (2016).
17. Prieto, J. Inflammation, HCC and sex: IL-6 in the centre of the triangle. *J. Hepatol.* **48**, 380–381. https://doi.org/10.1016/j.jhep.2007.11.007 (2008).
18. Jiang, J. *et al.* Hypoxia-induced HMGB1 expression of HCC promotes tumor invasiveness and metastasis via regulating macrophage-derived IL-6. *Exp. Cell Res.* **367**, 81–88. https://doi.org/10.1016/j.yexcr.2018.03.025 (2018).
19. Attia, Y. M., Tawfiq, R. A., Ali, A. A. & Elmazar, M. M. The FXR agonist, obeticholic acid, suppresses HCC proliferation & metastasis: Role of IL-6/STAT3 signalling pathway. *Sci. Rep.* **7**, 12502. https://doi.org/10.1038/s41598-017-12629-4 (2017).
20. Nakamura, H. & Takada, K. Reactive oxygen species in cancer: Current findings and future directions. *Cancer Sci.* **112**, 3945–3952. https://doi.org/10.1111/cas.15068 (2021).
21. Waris, G. & Ahsan, H. Reactive oxygen species: Role in the development of cancer and various chronic conditions. *J. Carcinog.* **5**, 14. https://doi.org/10.1186/1477-3163-5-14 (2006).

22. Ma, C. *et al.* NAFLD causes selective CD4(+) T lymphocyte loss and promotes hepatocarcinogenesis. *Nature* **531**, 253–257. https://doi.org/10.1038/nature16969 (2016).
23. Cheng, G., Cao, Z., Xu, X., van Meir, E. G. & Lambeth, J. D. Homologs of gp91phox: Cloning and tissue expression of Nox3, Nox4, and Nox5. *Gene* **269**, 131–140. https://doi.org/10.1016/s0378-1119(01)00449-8 (2001).
24. de Mochel, N. S. *et al.* Hepatocyte NAD(P)H oxidases as an endogenous source of reactive oxygen species during hepatitis C virus infection. *Hepatology* **52**, 47–59. https://doi.org/10.1002/hep.23671 (2010).
25. Boudreau, H. E., Emerson, S. U., Korzeniowska, A., Jendrysik, M. A. & Leto, T. L. Hepatitis C virus (HCV) proteins induce NADPH oxidase 4 expression in a transforming growth factor beta-dependent manner: A new contributor to HCV-induced oxidative stress. *J. Virol.* **83**, 12934–12946. https://doi.org/10.1128/JVI.01059-09 (2009).
26. Paik, Y. H. *et al.* Role of NADPH oxidases in liver fibrosis. *Antioxid. Redox Signal.* **20**, 2854–2872. https://doi.org/10.1089/ars.2013.5619 (2014).
27. Jiang, J. X. & Torok, N. J. NADPH oxidases in chronic liver diseases. *Adv. Hepatol.* **2014**, 742931. https://doi.org/10.1155/2014/742931 (2014).
28. Gabbia, D., Cannella, L. & De Martin, S. The role of oxidative stress in NAFLD-NASH-HCC transition-focus on NADPH oxidases. *Biomedicines* **9**, 687. https://doi.org/10.3390/biomedicines9060687 (2021).
29. Liang, S. *et al.* NADPH oxidase 1 in liver macrophages promotes inflammation and tumor development in mice. *Gastroenterology* **156**, 1156-1172.e6. https://doi.org/10.1053/j.gastro.2018.11.019 (2019).
30. Paik, Y. H. *et al.* The nicotinamide adenine dinucleotide phosphate oxidase (NOX) homologues NOX1 and NOX2/gp91(phox) mediate hepatic fibrosis in mice. *Hepatology* **53**, 1730–1741. https://doi.org/10.1002/hep.24281 (2011).
31. Penuelas-Haro, I. *et al.* The NADPH oxidase NOX4 regulates redox and metabolic homeostasis preventing HCC progression. *Hepatology* **78**, 416–433. https://doi.org/10.1002/hep.32702 (2023).
32. Ha, S. Y. *et al.* NADPH oxidase 1 and NADPH oxidase 4 have opposite prognostic effects for patients with hepatocellular carcinoma after hepatectomy. *Gut Liver* **10**, 826–835. https://doi.org/10.5009/gnl15543 (2016).
33. Dong, N. *et al.* M2 macrophages mediate sorafenib resistance by secreting HGF in a feed-forward manner in hepatocellular carcinoma. *Br. J. Cancer* **121**, 22–33. https://doi.org/10.1038/s41416-019-0482-x (2019).
34. Maeda, S., Kamata, H., Luo, J. L., Leffert, H. & Karin, M. IKKbeta couples hepatocyte death to cytokine-driven compensatory proliferation that promotes chemical hepatocarcinogenesis. *Cell* **121**, 977–990. https://doi.org/10.1016/j.cell.2005.04.014 (2005).
35. Choi, K. *et al.* The association of the serum levels of myostatin, follistatin, and interleukin-6 with sarcopenia, and their impacts on survival in patients with hepatocellular carcinoma. *Clin. Mol. Hepatol.* **26**, 492–505. https://doi.org/10.3350/cmh.2020.0005 (2020).
36. Wong, V. W. *et al.* High serum interleukin-6 level predicts future hepatocellular carcinoma development in patients with chronic hepatitis B. *Int. J. Cancer* **124**, 2766–2770. https://doi.org/10.1002/ijc.24281 (2009).
37. Crosas-Molist, E. *et al.* The NADPH oxidase NOX4 inhibits hepatocyte proliferation and liver cancer progression. *Free Radic. Biol. Med.* **69**, 338–347. https://doi.org/10.1016/j.freeradbiomed.2014.01.040 (2014).
38. Lan, T., Kisseleva, T. & Brenner, D. A. Deficiency of NOX1 or NOX4 prevents liver inflammation and fibrosis in mice through inhibition of hepatic stellate cell activation. *PLoS ONE* **10**, e0129743. https://doi.org/10.1371/journal.pone.0129743 (2015).
39. Lu, Y. *et al.* Resident immune cells of the liver in the tumor microenvironment. *Front. Oncol.* **12**, 931995. https://doi.org/10.3389/fonc.2022.931995 (2022).
40. Li, X. *et al.* Landscape of immune cells heterogeneity in liver transplantation by single-cell RNA sequencing analysis. *Front. Immunol.* **13**, 890019. https://doi.org/10.3389/fimmu.2022.890019 (2022).
41. Zhang, Q. *et al.* Landscape and dynamics of single immune cells in hepatocellular carcinoma. *Cell* **179**, 829-845.e20. https://doi.org/10.1016/j.cell.2019.10.003 (2019).
42. Zhang, J. *et al.* Tumoral NOX4 recruits M2 tumor-associated macrophages via ROS/PI3K signaling-dependent various cytokine production to promote NSCLC growth. *Redox Biol.* **22**, 101116. https://doi.org/10.1016/j.redox.2019.101116 (2019).
43. Chaudhry, S., Emond, J. & Griesemer, A. Immune cell trafficking to the liver. *Transplantation* **103**, 1323–1337. https://doi.org/10.1097/TP.0000000000002690 (2019).
44. Robinson, M. W., Harmon, C. & O'Farrelly, C. Liver immunology and its role in inflammation and homeostasis. *Cell. Mol. Immunol.* **13**, 267–276. https://doi.org/10.1038/cmi.2016.3 (2016).
45. Krenkel, O. & Tacke, F. Liver macrophages in tissue homeostasis and disease. *Nat. Rev. Immunol.* **17**, 306–321. https://doi.org/10.1038/nri.2017.11 (2017).
46. Tacke, F. Targeting hepatic macrophages to treat liver diseases. *J. Hepatol.* **66**, 1300–1312. https://doi.org/10.1016/j.jhep.2017.02.026 (2017).
47. Dong, X., Liu, J., Xu, Y. & Cao, H. Role of macrophages in experimental liver injury and repair in mice. *Exp. Ther. Med.* **17**, 3835–3847. https://doi.org/10.3892/etm.2019.7450 (2019).
48. Ricketts, T. D., Prieto-Dominguez, N., Gowda, P. S. & Ubil, E. Mechanisms of macrophage plasticity in the tumor environment: Manipulating activation state to improve outcomes. *Front. Immunol.* **12**, 642285. https://doi.org/10.3389/fimmu.2021.642285 (2021).
49. Boutilier, A. J. & Elsawa, S. F. Macrophage polarization states in the tumor microenvironment. *Int. J. Mol. Sci.* **22**, 6995. https://doi.org/10.3390/ijms22136995 (2021).
50. Yao, Y., Xu, X. H. & Jin, L. Macrophage polarization in physiological and pathological pregnancy. *Front. Immunol.* **10**, 792. https://doi.org/10.3389/fimmu.2019.00792 (2019).
51. Kouketsu, A. *et al.* Regulatory T cells and M2-polarized tumour-associated macrophages are associated with the oncogenesis and progression of oral squamous cell carcinoma. *Int. J. Oral Maxillofac. Surg.* **48**, 1279–1288. https://doi.org/10.1016/j.ijom.2019.04.004 (2019).
52. Fu, X. H. *et al.* M2-macrophage-derived exosomes promote meningioma progression through TGF-beta signaling pathway. *J. Immunol. Res.* **2022**, 8326591. https://doi.org/10.1155/2022/8326591 (2022).
53. Chen, X. J. *et al.* Clinical significance of CD163+ and CD68+ tumor-associated macrophages in high-risk HPV-related cervical cancer. *J. Cancer* **8**, 3868–3875. https://doi.org/10.7150/jca.21444 (2017).

Acknowledgements

This research was supported by a grant of the Korea Health Technology R&D Project through the Korea Health Industry Development Institute (KHIDI), funded by the Ministry of Health & Welfare, Republic of Korea (HI19C1328, JYKHR20C0025, YHP) and the National Research Foundation of Korea (NRF) grant funded by the Ministry of Science and ICT (MSIT) of Korea (NRF-2017R1A2B2002735, YHP; NRF-2019R1C1C1007729, WK). This study was also supported by Future Medicine 20*30 Project of the Samsung Medical Center (#SMX1240011, WK).

Author contributions

JYK, WK and YHP designed the study. JYK, SY and SHP carried out the experiments. JYK, SYH, WK and YHP

analyzed and interpreted the data. JYK, WK and YHP wrote the original draft. WK and YHP revised the paper. All authors approved the final version of the manuscript.

Competing interests
The authors declare no competing interests.

Additional information
Supplementary Information The online version contains supplementary material available at https://doi.org/10.1038/s41598-024-72721-4.

Correspondence and requests for materials should be addressed to Y.-H.P.

Reprints and permissions information is available at www.nature.com/reprints.

Publisher's note Springer Nature remains neutral with regard to jurisdictional claims in published maps and institutional affiliations.